AMERICAN SOCIETY FOR MICROBIOLOGY | Journal of Virology®

CELLULAR RESPONSE TO INFECTION

Ulk1 Governs Nerve Growth Factor/TrkA Signaling by Mediating Rab5 GTPase Activation in Porcine Hemagglutinating Encephalomyelitis Virus-Induced Neurodegenerative Disorders

Zi Li,[a] Kui Zhao,[a] Xiaoling Lv,[a] Yungang Lan,[a] Shiyu Hu,[a] Junchao Shi,[a] Jiyu Guan,[a] Yawen Yang,[a] Huijun Lu,[b] Hongbin He,[c] Feng Gao,[a] Wenqi He[a]

[a]Key Laboratory of Zoonosis Research, Ministry of Education, College of Veterinary Medicine, Jilin University, Changchun, China

[b]Key Laboratory of Zoonosis Research, Ministry of Education, Institute of Zoonosis, Jilin University, Changchun, China

[c]Key Laboratory of Animal Resistant Biology of Shandong, Ruminant Disease Research Center, College of Life Sciences, Shandong Normal University, Jinan, China

ABSTRACT Porcine hemagglutinating encephalomyelitis virus (PHEV) is a highly neurovirulent coronavirus and causes neurological dysfunction in the central nervous system (CNS), but the neuropathological mechanism of PHEV remains poorly understood. We report that Unc51-like kinase 1 (Ulk1/Unc51.1) is a pivotal regulator of PHEV-induced neurological disorders and functions to selectively control the initiation of nerve growth factor (NGF)/TrkA endosome trafficking. We first identified the function of Ulk1 by histopathologic evaluation in a PHEV-infected mouse model in which neuronal loss was accompanied by the suppression of Ulk1 expression. Morphogenesis assessments in the primary cortical neurons revealed that overexpression or mutations of Ulk1 modulated neurite outgrowth, collateral sprouting, and endosomal transport. Likewise, Ulk1 expression was decreased following PHEV infection, suggesting that there was a correlation between the neurodegeneration and functional Ulk1 deficiency. We then showed that Ulk1 forms a multiprotein complex with TrkA and the early endosome marker Rab5 and that Ulk1 defects lead to either blocking of NGF/TrkA endocytosis or premature degradation of pTrkA via constitutive activation of the Rab5 GTPase. Further investigation determined that the ectopic expression of Rab5 mutants induces aberrant endosomal accumulation of activated pTrkA, proving that targeting of Ulk1-TrkA-NGF signaling to the retrograde transport route in the neurodegenerative process that underlies PHEV infection is dependent on Rab5 GTPase activity. Therefore, we described a long-distance signaling mechanism of PHEV-driven deficits in neurons and suggested that such Ulk1 repression may result in limited NGF/TrkA retrograde signaling within activated Rab5 endosomes, explaining the progressive failure of neurite outgrowth and survival.

IMPORTANCE Porcine hemagglutinating encephalomyelitis virus (PHEV) is a neurotropic coronavirus and targets neurons in the nervous system for proliferation, frequently leaving behind grievous neurodegeneration. Structural plasticity disorders occur in the axons, dendrites, and dendritic spines of PHEV-infected neurons, and dysfunction of this neural process may contribute to neurologic pathologies, but the mechanisms remain undetermined. Further understanding of the neurological manifestations underlying PHEV infection in the CNS may provide insights into both neurodevelopmental and neurodegenerative diseases that may be conducive to targeted approaches for treatment. The significance of our research is in identifying an Ulk1-related neurodegenerative mechanism, focusing on the regulatory functions of Ulk1 in the transport of long-distance trophic signaling endosomes, thereby explaining the progressive failure of neurite outgrowth and survival associated with PHEV

Received 27 February 2018 **Accepted** 25 May 2018

Accepted manuscript posted online 6 June 2018

Citation Li Z, Zhao K, Lv X, Lan Y, Hu S, Shi J, Guan J, Yang Y, Lu H, He H, Gao F, He W. 2018. Ulk1 governs nerve growth factor/TrkA signaling by mediating Rab5 GTPase activation in porcine hemagglutinating encephalomyelitis virus-induced neurodegenerative disorders. J Virol 92:e00325-18. https://doi.org/10.1128/JVI.00325-18.

Editor Julie K. Pfeiffer, University of Texas Southwestern Medical Center

Address correspondence to Wenqi He, hewq@jlu.edu.cn.

Z.L. and K.Z. contributed equally to this article.

aggression. This is the first report to define a mechanistic link between alterations in signaling from endocytic pathways and the neuropathogenesis of PHEV-induced CNS disease.

KEYWORDS NGF, porcine hemagglutinating encephalomyelitis virus, Rab5, Ulk1, neurodegeneration, neurovirulent coronavirus

Porcine hemagglutinating encephalomyelitis virus (PHEV) is a nonsegmented, positive-sense RNA virus of the family *Coronaviridae*. The virus was first isolated from the brains of suckling pigs in 1962 and causes encephalomyelitis and/or vomiting and wasting disease (VWD) in piglets (1, 2). So far, the infection has been reported in the major pig-raising countries of Europe, Asia, and North America, where the overall mortality rate of suffering piglets under 3 weeks of age ranged from 30% to 100% (3–6). PHEV propagates via neural circuits to the central nervous system (CNS) after peripheral inoculation, resulting in acute deadly encephalomyelitis and neurological dysfunction in younger rats (7). Immunohistochemically, viral antigen has been detected in the brain, spinal cord, and dorsal root ganglia. Subsequent studies have demonstrated that PHEV hijacks host endocytosis to enter into neural cells, and endo-/exocytosis can be used for transsynaptic transfer of the virus (8, 9). Most recently, there have been acute outbreaks of influenza-like illness (ILI) in swine in Michigan, USA, and testing identified PHEV as the cause of the disease (10). The ILI uncovered here may reflect an atypical form of disease or a form of PHEV with increased virulence.

Viral etiology has been postulated in several neurodegenerative diseases and provides insight into potential host- and pathogen-dependent mechanisms involved in the disease process. Infection by neurotropic viruses, including Theiler's murine encephalomyelitis virus (TMEV), herpes simplex virus (HSV), rabies virus, and influenza virus, can irreversibly disrupt the complex structural and functional architecture of the CNS, frequently leaving behind grievous neurodegeneration or a fatal prognosis (11–13). Among them, neurotropic strains of mouse hepatitis virus (MHV) have been widely used as models for the study of the human demyelination and neurodegeneration resembling multiple sclerosis (MS) pathology (14, 15). Likewise, PHEV is a neurotropic virus and belongs to the genus *Betacoronavirus*, along with MHV, and is associated with a wide spectrum of neuropathological changes in susceptible animals, supporting a causal link between PHEV and neurodegenerative disorders.

Many neurodegenerative diseases occur as a result of neurodegeneration processes, where the progressive loss of structure or functions of neurons is commonly found (16, 17). Structural plasticity occurs in the axons, dendrites, and dendritic spines, identifying adaptive/homeostatic neural processes in the nervous system, and dysfunction of this process may contribute to neurologic pathologies. In PHEV-induced CNS disease, global screening of differentially expressed genes has identified the downregulation of expression of the serine/threonine kinase Ulk1 (18). Apart from its essential role in initiating autophagy, Ulk1 works as a regulatory protein that participates in phylogenetically conserved pathways involving neurite formation, synaptic transmission, and endocytic trafficking during CNS development in *Caenorhabditis elegans* and mammals (19–22). Large families of structurally related motor proteins and transport components have been identified as binding partners of Ulk1, and they are cooperatively involved in trophic factor receptor internalization, signal transduction, and intracellular vesicular turnover (19, 20, 23). In addition, these steps depend on small Rab GTPases, such as Rab5, which is a rate-limiting component of the machinery that regulates the kinetics of membrane traffic in the early endocytic pathway. A population of Rab5-positive signaling endosomes containing endocytosed nerve growth factor (NGF) complex controls the speed of axon elongation in developing neurons (24, 25). Therefore, a noncanonical or evolutionarily conserved role for Ulk1 may indicate a link between endocytosis and neuronal survival, and the dysfunction of Ulk1 may be implicated in the pathogenesis of various neurodegenerative disorders (21, 26).

Although multiple factors may also contribute to the neuropathology of PHEV

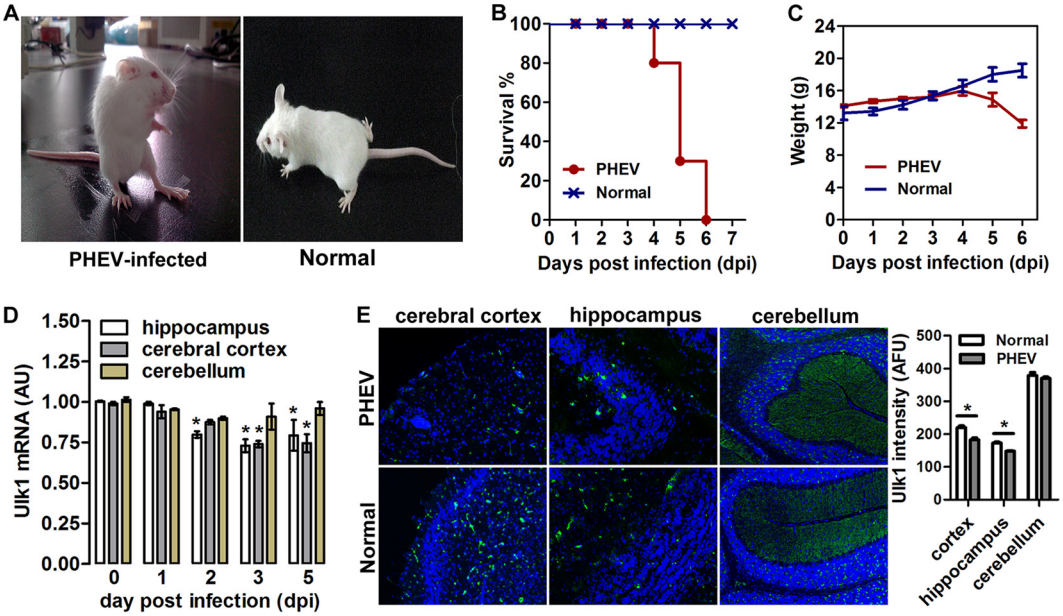

FIG 1 Decreased Ulk1 expression in the CNS of PHEV-infected mice. (A) Mice that were intranasally inoculated with 100 μl PHEV ($10^{4.45}$ $TCID_{50}$/0.1 ml) showed typical neurological symptoms at 3 dpi, such as abnormal gait, tremors, listlessness, standing upright, raised forelimbs, and arched waists. Mice in the control group survived normally. (B) Survival curves of PHEV-infected mice (n = 10 mice per group; data from three independent experiments). (C) Body weight curves of PHEV-infected and control mice from 0 to 6 dpi. From 4 dpi, PHEV-infected mice exhibited a significantly lesser body weight than that observed in the control mice. (D) qRT-PCR analysis of Ulk1 mRNA levels in mouse brain after PHEV infection. Data are presented as the means ± standard errors of the means (SEM) (n = 6). (E) *In situ* hybridization of the mouse brain for Ulk1 mRNA (green) with an antisense probe. Quantitative analysis is summarized in the histograms on the right. The *y* axis is the average Ulk1 mRNA intensity in arbitrary fluorescence units.

infection, the above-mentioned evidence offers new insight into an Ulk1-related neurodegenerative mechanism. We investigated the functional significance of Ulk1 during PHEV infection, focusing on its regulatory functions in the transport of long-distance trophic signaling endosomes. Thereby, we revealed that Ulk1 dysfunction results in limited NGF/TrkA retrograde signaling within activated Rab5 endosomes, explaining the progressive failure of neurite outgrowth and survival in PHEV-infected neurons. Most notably, a better understanding of the mechanisms underlying the neurological manifestations of PHEV-induced CNS disease that may be expected to provide tools for exploring more-effective intervention strategies and treatment regimens of neurodegenerative disorders was gained.

RESULTS

Mice lacking Ulk1 expression exhibit neuronal loss in the CNS. Ulk1 is known mainly for its regulatory role in autophagy in response to nutrient deprivation, whereas little research has focused on its function in nervous system disease. To investigate the role of Ulk1 in neurodegenerative disease, 3-week-old BALB/c mice were inoculated intranasally with PHEV and monitored daily for clinical symptoms. Neurologic signs, such as abnormal gait, tremors, dullness, listlessness, standing, raised forelimbs, arched waists, and nystagmus were observed in the infected mice at 2 to 3 days postinoculation (dpi) (Fig. 1A). Survival times were shorter in PHEV-infected mice than in control group mice, and all the infected mice had a significantly lesser body weight starting at 4 dpi and died over the ensuing a week (Fig. 1B and C). We confirmed a decrease of Ulk1 expression in the brain (i.e., the cerebral cortex, hippocampal formation) of infected mice by quantitative reverse transcription-PCR (qRT-PCR) analyses (Fig. 1D). Using *in situ* hybridization (ISH) from histological sections of mouse brain, we revealed that Ulk1 mRNA was expressed throughout the CNS, with the highest levels in the hippocampus, prefrontal cortex, and cerebellum (Fig. 1E). The expression density map

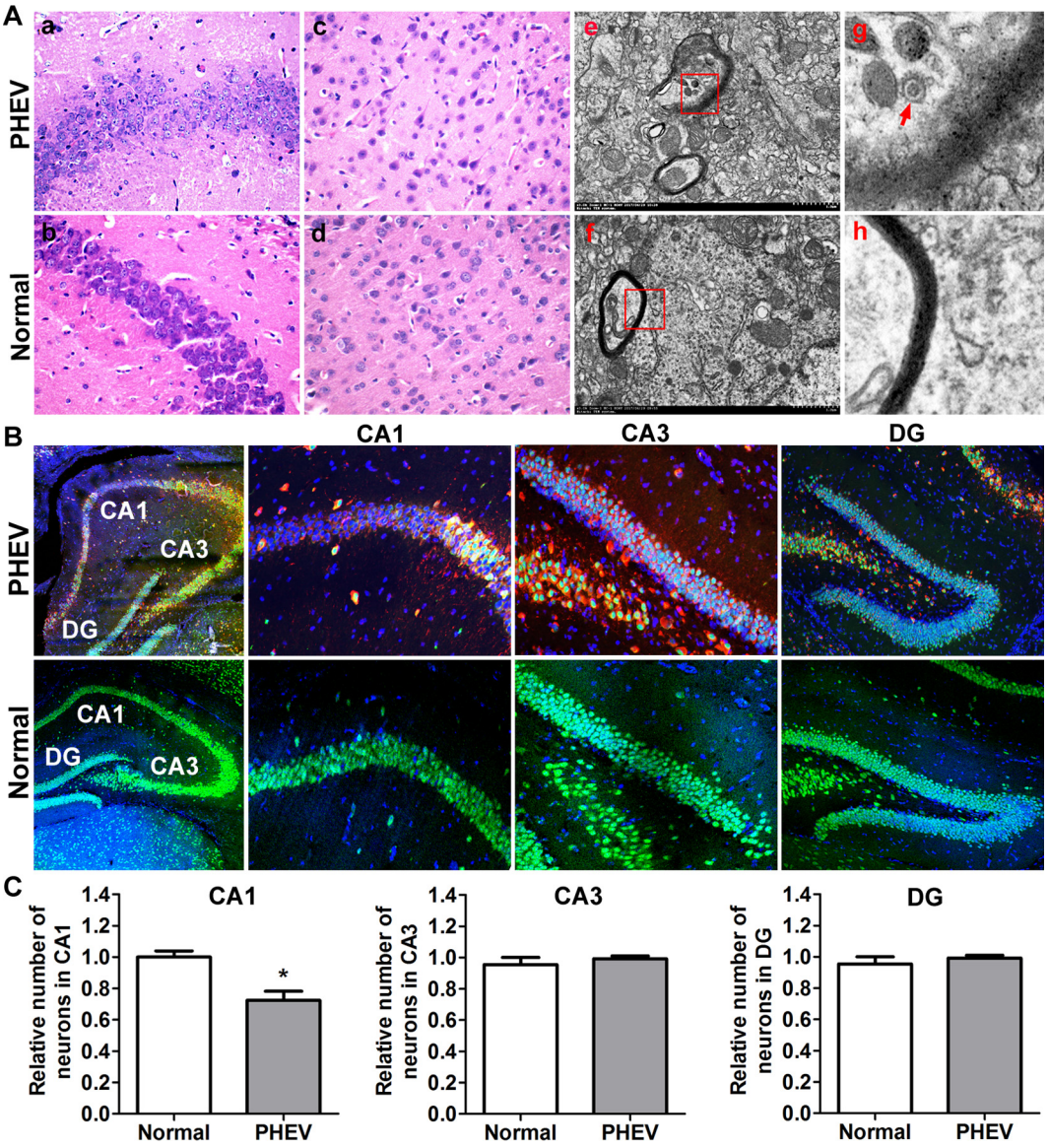

FIG 2 Degeneration of neurons in the CNS of PHEV-infected mice. (A) Serial mouse brain sections stained with H&E demonstrated the loss of pyramidal neurons in the PHEV-infected mice (a to d). Ultrathin sections from mouse brain that were stained with uranyl acetate and lead citrate showed myelin degeneration (e to h). The arrow indicates a PHEV particle. (B) Representative images of serial brain sections (hippocampal areas CA1, CA3, and dentate gyrus [DG]) stained with DAPI (blue) and antibodies against the neuronal markers NeuN (green) and PHEV (red). (C) Average number of neurons (normalized to that in uninfected controls) ± SEM in the indicated area ($n = 3$ mice). *, $P < 0.05$ (Student's t test).

also indicated that, in the PHEV-infected mouse brain, Ulk1 expression was suppressed in specific regions, notably, in regions with high structural plasticity, implying that the decrease of Ulk1 expression may be related to context-dependent CNS dysfunction during PHEV infection.

To identify the neurologic deficits in these mice, we analyzed their brain histology at various time points. Hematoxylin and eosin (H&E) staining showed progressive degeneration of pyramidal neurons, including neuronal loss and loosely arranged neurons, a serious lack of cytoplasmic staining shades, and absent or not obvious nucleoli, in the hippocampal CA1 and cerebral cortical regions after PHEV invasion (Fig. 2A, panels a to d). These results were confirmed at the ultrastructural level, where representative foci of progressive myelin degeneration and axonal damage were selected from high-resolution transmission electron microscopy (TEM) images, indicat-

ing a possible degenerating process (Fig. 2A, panels e to h). The integrity of the hippocampal matter was evaluated during PHEV infection by assessing the number of pyramidal neurons using ImageJ. As hypothesized, the number of nondamaged neurons (as identified by NeuN/4′,6-diamidino-2-phenylindole [DAPI] colabeling of pyramidal neurons) within CA1 in PHEV-infected mice was significantly smaller than that in the healthy controls (Fig. 2B and C). These findings suggest that PHEV attacks mainly neurons in the CNS and induces neurodegeneration, and mice lacking Ulk1 expression in the CNS are likely to be associated with neurologic deficits.

Ulk1-deficient control of neuronal degeneration *in vitro*. Since Ulk1 was determined to be correlated with the CNS degeneration in the PHEV-infected mice, we next tested whether the pivotal function of Ulk1 was already impaired in the primary cultural rat cortical neurons in an *in vitro* system. At 5 days *in vitro* (DIV), the primary cortical neurons were infected with PHEV at a multiplicity of infection (MOI) of 50, and we confirmed that the level of endogenous Ulk1 was decreased during PHEV infection by using qRT-PCR and Western blot assessments (Fig. 3A). To investigate whether Ulk1 deficiency was the primary cause of neuronal degeneration underlying PHEV infection, we then applied the clustered regularly interspaced short palindromic repeat(s)-associated protein-9 nuclease (CRISPR/Cas9) system to modify the Ulk1 gene at the DNA level. For targeting the endogenous Ulk1 gene, two small-guide RNAs (sgRNAs) were designed and cloned into a pSpCas9 (BB)-2A-Puro vector (abbreviated as Ulk1-pSpCas9) (Fig. 3B). Ulk1-pSpCas9 was then transfected into primary cortical neurons at 4 DIV. After 24 to 72 h of culture with puromycin screening, about 37.5% of transfected neurons carried the puromycin resistance gene and survived, and their genomic DNA was extracted for the PCR assay. Using the T7E1 assay and PCR Sanger sequencing, we discovered around 44.4% (4/9) of efficient mutations in the Ulk1 gene (Fig. 3B and C). Likewise, Western blot analysis revealed that the Ulk1 protein expression was suppressed 3- to 5-fold at 48 h ($P < 0.01$) and 6- to 12-fold at 72 h ($P < 0.01$) in these transfected neurons (Fig. 3D), suggesting that the CRISPR-Cas9-mediated Ulk1 knockout was efficient in this study. We then employed immunological examinations with microtubule-associated protein 2 (MAP2) staining and found that in the normal neurons, Ulk1 had a punctuated, vesicular distribution pattern along the axon shaft and dendritic branches, particularly at the branching points and dendritic spines, suggesting the possible involvement of Ulk1 in neuronal endosomal trafficking (Fig. 3E). During PHEV infection, Ulk1 expression was reduced and the distribution pattern of Ulk1 was disrupted, mainly by blockage within the axon shaft, implying a transport disorder (Fig. 3E). Antibody staining in the Ulk1-pSpCas9-transfected neurons also revealed that all of these surviving Ulk1 mutant neurons exerted multiple neurite deficits, including irregular dendritic and axonal swelling, disconnected axons, reduced dendritic branches, absence of dendritic spines, and an abnormal accumulation of Ulk1 protein in the neuritic beading. These are early hallmarks of neuronal degeneration and consistent with the expected defects that occur during PHEV infection (Fig. 3E). This aberrant morphological phenotype in Ulk1 mutants helped to validate our finding that Ulk1 deficiency was probably the primary cause of neuronal degeneration induced by PHEV.

To learn the role of Ulk1 in PHEV-induced dendrite arborization, we therefore overexpressed replication-deficient adenovirus-based green fluorescent protein expression vectors encoding Ulk1 (Ad-GFP-Ulk1) in cortical neurons that were preincubated with PHEV. At 48 h posttransfection, the expression of Ulk1 in Ad-GFP-Ulk1-transfected neurons was significantly increased compared with that of the Ad-GFP-transfected or untreated neurons (Fig. 3F). Representative micrographs showed strengthened neurite outgrowth and regeneration in these injured neurons, indicating that the defective neuronal morphogenesis was rescued by the gain of function of Ulk1 (Fig. 3G). Without rescue, PHEV-infected neurons, in contrast, exhibited progressive degeneration, i.e., stunted axon elongation, axonotmesis, disintegrated dendritic outgrowths, excessive axon arborization, and numerous irregular membrane-walled cisternae inside the terminals (Fig. 3G). Quantitative analyses of these phenotypes are summarized in a

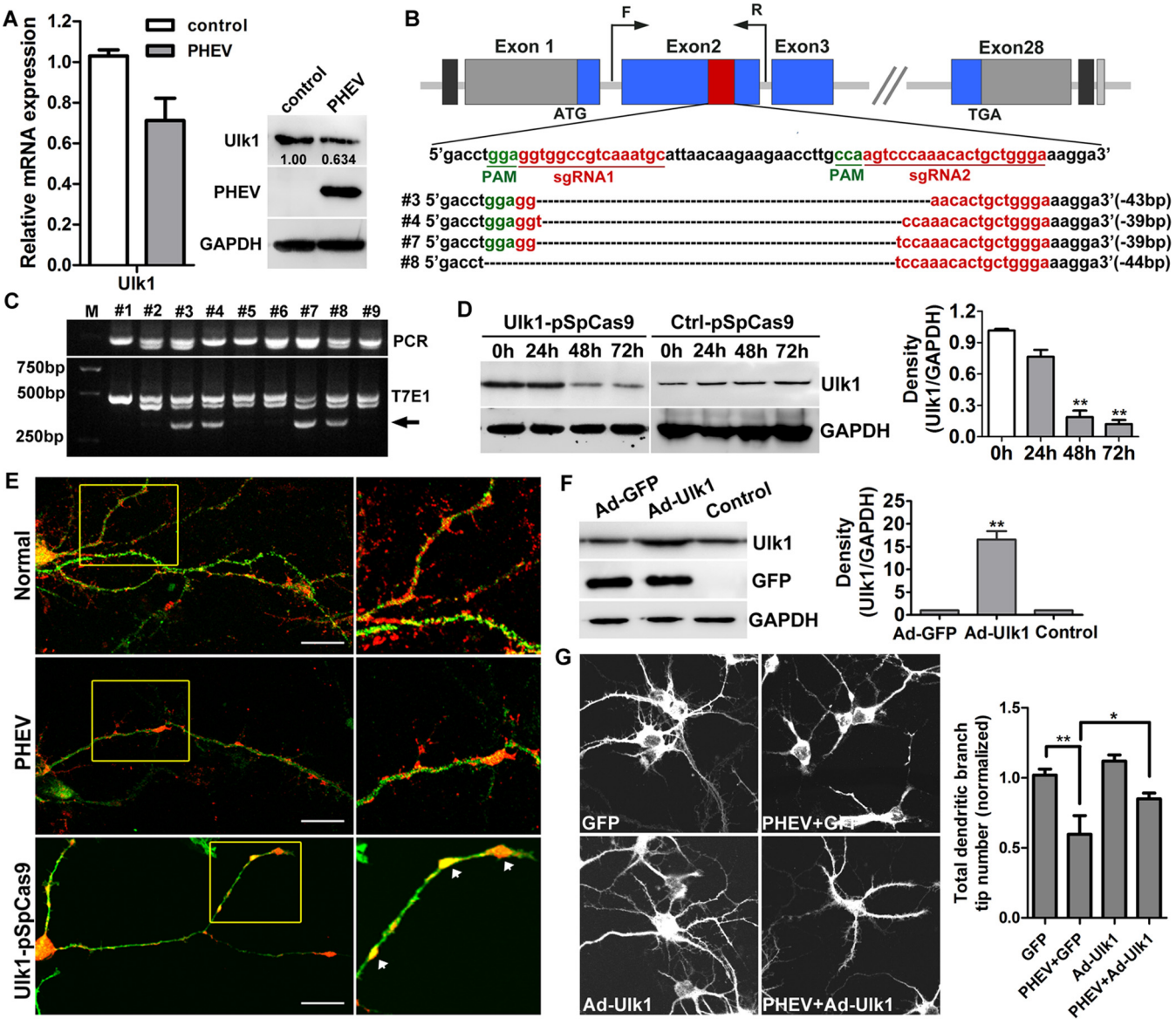

FIG 3 Ulk1 deficiency in cortical neurons is associated with PHEV-induced degeneration. (A) The suppression of Ulk1 in the cortical neurons that were preincubated with PHEV was verified by qRT-PCR and Western blotting. The levels of Ulk1 expression were normalized to the uninfected controls. Anti-Ulk1 antibodies were used to determine the level of Ulk1 and mouse anti-GAPDH antibody to determine protein loading. *, $P < 0.05$ (Student's *t* test). (B) CRISPR/Cas9-mediated gene targeting of Ulk1 in cortical neurons. Schematic diagram of sgRNA targeting the Ulk1 gene loci (top panel) and Sanger sequencing of the modified Ulk1 alleles (bottom panel). (C) The target fragments were amplified by PCR from genomic DNA that was extracted from independent transgenic neurons, and detection of target mutations was performed by T7E1 cleavage assay. M, DL2000; #1 to #9 represent 9 independent transgenic Ulk1 sgRNAs neurons. Arrows indicate the fragments digested by T7E1. (D) Cortical neurons at 4 DIV were transfected with Ctrl-pSpCas9 or Ulk1-pSpCas9. Western blot analysis confirmed that Ulk1 protein was significantly decreased in these knockdown neurons. Relative protein levels were analyzed by using ImageJ software. (E) In the transgenic group, cortical neurons at 4 DIV were transfected with Ulk1-pSpCas9, followed by puromycin screening for a total of 48 h. In the infected group, cortical neurons at 5 DIV were incubated with PHEV for 24 h. The expression and localization of Ulk1 were determined by antibody staining using antibodies against Ulk1 (1:100, red) and MAP2 (1:100, green). The boxed insets are shown at a greater magnification in the panels on the right. Neuritic beading or focal beadlike swellings in the dendrites and axons are indicated by arrows. Bars, 50 μm. (F) The primary cortical neurons were transfected with Ad-GFP-Ulk1 or Ad-GFP at an MOI of 100. Forty-eight hours after transfection, the cells were harvested for analysis of Western blots. Relative protein levels were analyzed by using ImageJ software. (G) Cortical neurons at 5 DIV were incubated with PHEV for 24 h and were then transfected with Ad-GFP or Ad-GFP-Ulk1 for 48 h. Representative images are shown. Histograms show the normalized total dendritic branch tip number. The mean values from the Ad-GFP-transfected neurons were set at 1.0. Data are shown as the means ± SEM from the three experiments. The numbers in the histograms indicate the neuron numbers from the three experiments. *, $P < 0.05$; **, $P < 0.01$ (Student's *t* test).

histogram (Fig. 3G). These results reveal the critical role of Ulk1 in the facilitation of growing neurons.

Loss of Ulk1 contributes to NGF/TrkA signal defects in PHEV-infected neurons. We next explored the possible mechanisms underlying the neuronal degeneration that

was associated with Ulk1 modest loss during PHEV infection. Previous research has revealed that p62 and Ulk1 are recruited to the NGF high-affinity receptor TrkA to regulate NGF/TrkA endocytosis (21). This trophic signal is necessary for axonal arbor expansion and collateral sprouting, which relies on multiple effector cascades to transduce contextual information and generate the appropriate responses. Consistent with our above-reported findings, we presumed it was possible that the disorder phenotypes in PHEV-infected neurons were caused by the dysfunction of Ulk1-mediated NGF/TrkA retrograde signaling. To test this possibility, primary cortical neurons were incubated with PHEV and detected by Western blot analysis. We found that Ulk1 expression was inhibited in the PHEV-infected cortical neurons and that the active form of TrkA (phosphorylated TrkA [pTrkA]) was preferentially decreased, whereas there was a steady-state, basal level of TrkA (Fig. 4A). We then used a Cy3-conjugated NGF-based endocytosis assay to achieve efficient internalization of NGF. Ulk1 mutant neurons, PHEV-infected neurons, and Ad-Ulk1-transfected neurons were first cultured for 48 h in the presence of 1 nM unlabeled NGF, and then the culture medium was replaced with fresh medium containing 10 nM Cy3-NGF and incubated for 10 min. Afterward, the ability of these neurons to take up fluorescence-labeled NGF was scored by a flow cytometry assay (fluorescence-activated cell sorting [FACS]), and we determined that the internalization ratio of NGF obtained for the mutant and infected neurons decreased by 54.25% and 41.55%, respectively (Fig. 4B). At this point, the internalization ratio in the Ad-Ulk1-transfected neurons was not significantly changed (Fig. 4B). These results were confirmed by a microscopic assay, and a faint Cy3-fluorescent signal was detected in PHEV-infected or Ulk1 mutant neurons, indicating a severe NGF deficiency in the cortical neurons (Fig. 4C).

To test whether these morphology changes were dependent on NGF endocytosis, we performed a neurite outgrowth assay. NGF (10 nM) was directly added to the culture at various times, and we found that a high concentration of NGF increased TrkA phosphorylation and that Ulk1 continuously increased despite PHEV infection (Fig. 5A). Importantly, in the PHEV-infected neurons, stimulation with NGF was associated with more-significant growth and fewer neuritic beadings, and some stalled spines tended to develop normally into mature spines, although this effect was limited (Fig. 5B). Similarly, the NGF stimulation strategy appeared to rescue the aberrant development in the Ulk1 mutant neurons (Fig. 5B), suggesting that NGF internalization is required for Ulk1-dependent production of neurite growth. Together, these findings indicated that PHEV functionally suppressed Ulk1 expression, thereby contributing to NGF/TrkA retrograde signaling defects.

Multiprotein complex of Ulk1 and TrkA present in Rab5 endosomes. NGF induces neurite outgrowth and differentiation in a process that involves endocytosis of the NGF/TrkA complex into signaling endosomes. The early endosomal marker Rab5 has been observed to be associated with signaling endosomes and involved in long-distance retrograde transport of NGF in axons, and Rab5 activity needs to be suppressed at this stage to avoid fusion with conventional early endosomes for lysosomal degradation (27). Therefore, we transfected enhanced GFP (EGFP)-tagged Rab5 into the cultured cortical neurons, followed by PHEV infection, and sought to determine whether Ulk1-mediated NGF/TrkA retrograde transport was associated with Rab5 endosomes. Microscopy data detected some diffuse punctate signals of the Rab5 endosomes in the normal neurons (Fig. 6A). Comparatively, in the PHEV-infected neurons, increasing numbers of ectopic punctate signals of Rab5 endosomes that were more heterogeneous in size and had irregular accumulations were observed (Fig. 6A). Meanwhile, EGFP-Rab5-expressing axons were stained to visualize Ulk1 and pTrkA expression, and we found that both Ulk1 and pTrkA colocalized with Rab5 endosomes in growing axons, implying that the majority of the Ulk1/pTrkA pool is associated with Rab5 (Fig. 6B). This prompted us to hypothesize that PHEV controls the retrograde trafficking of Ulk1/pTrkA complexes via the Rab5 endosomal system. To dissect whether the spatial association was also reflected in protein-protein binding, Rab5-containing

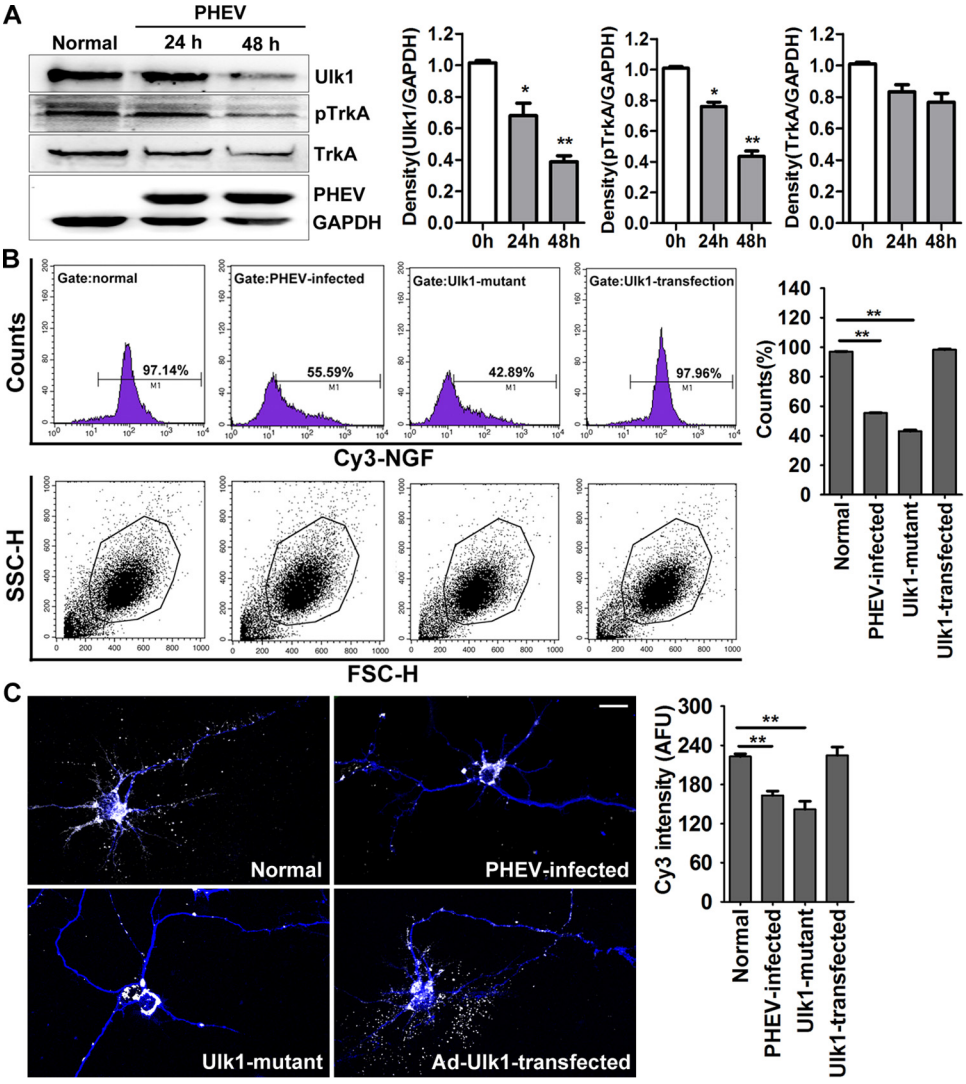

FIG 4 PHEV infection suppresses the Ulk1-mediated endocytosis of NGF/TrkA complexes. (A) Cortical neurons were incubated with PHEV as indicated, and cell lysates were analyzed by Western blotting with antibodies against Ulk1, TrkA, pTrkA, PHEV, and GAPDH. Ulk1 and pTrkA expression were inhibited by PHEV, although the total expression of TrkA was not significantly affected. Densitometric analysis was performed; Ulk1, pTrkA, and TrkA intensities were normalized against the amount of GAPDH. (B) Cy3-NGF internalization assay: Cy3-NGF in the Ad-GFP-Ulk1-transfected, Ulk1 mutant, PHEV-infected, and normal cortical neurons was detected by FACS, and the data were normalized to internalization rates in normal neurons. Representative FACS profiles obtained during the analysis are shown, and Cy3 signals were gated in M1 and expressed as a percentage of the total number of cells analyzed. SSC-H, side scatter height; FSC-H, forward scatter height. (C) Representative images of Cy3-NGF (white) internalization in the MAP2-marked neurons (blue). Quantitative analyses revealed that the Cy3-NGF internalization was markedly suppressed in the PHEV-infected or Ulk1 mutant neurons. The *y* axis represents the average Cy3 intensity using arbitrary fluorescence units. Bars, 20 μm. *, $P < 0.05$; **, $P < 0.01$ (Student's *t* test).

complexes were immunoprecipitated from homogenized cell lysates that were either treated or not treated with PHEV, and then the profiles of pTrkA and Ulk1 were determined by immunoblot analysis. We found that both pTrkA and Ulk1 coimmunoprecipitated with Rab5 at low but detectable levels, and the degree of association was significantly weakened by a mean of 62% ($P < 0.034$) after PHEV stimulation (Fig. 6C). Otherwise, modulating Ulk1 expression in the cortical neurons with transfection by Ad-GFP-Ulk1 and Ulk1-pSpCas9 induced changes in pTrkA level that were positively correlated with Ulk1, demonstrating a formation of these traffic-related protein complexes (Fig. 6D). These results were consistent with the spatial association based on the coimmunoprecipitation (co-IP) assay and supported the finding that Ulk1 cross talk

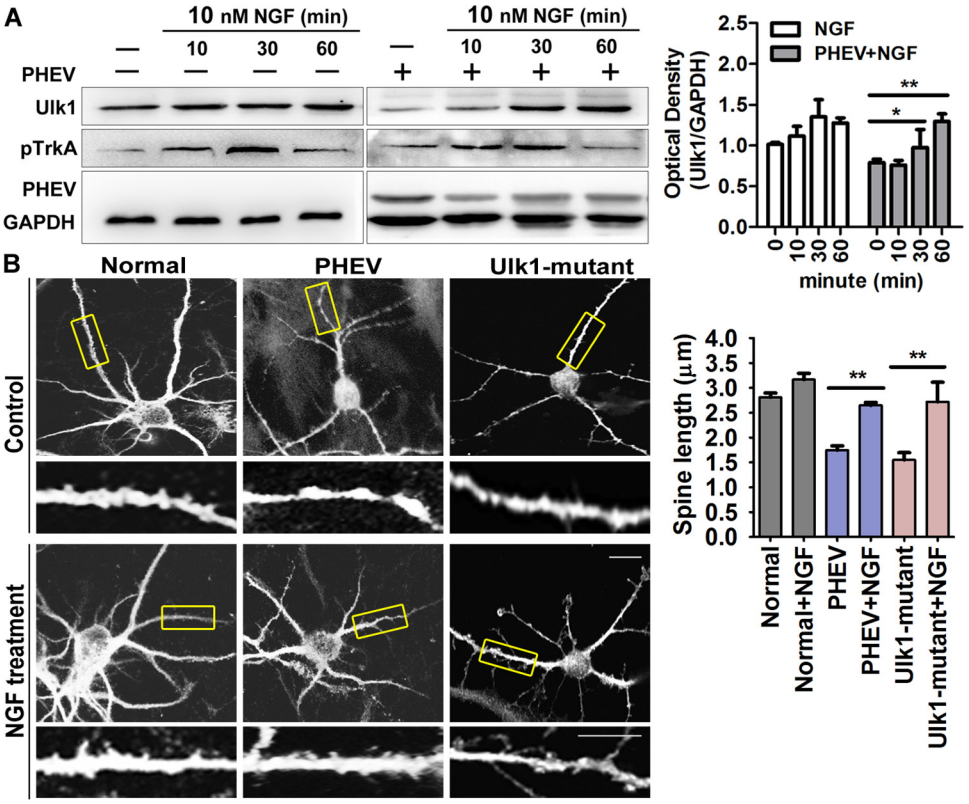

FIG 5 NGF internalization is required for Ulk1-dependent production of neurite morphogenesis. (A) Time course of NGF-stimulated phosphorylation of TrkA. Neurons were stimulated with 10 nM NGF for different amounts of time (0, 10, 30, and 60 min) and lysed. Then, Western blotting was used to check for Ulk1, pTrkA, and GAPDH expression. TrkA was maximally phosphorylated within 30 min after adding NGF. Densitometric analysis was performed, and Ulk1 intensities were normalized against GAPDH. (B) Cortical neurons were preincubated with PHEV at 5 DIV for 24 h or pretransfected with Ulk1-pSpCas9 at 4 DIV for 48 h, followed by being treated with 10 nM NGF. After 24 h, these neurons were stained for MAP2; representative micrographs are shown. The bottom panels (insets of boxed areas) show high-magnification images of shorter spines. Bars, 20 μm (top images) or 5 μm (high-magnification images). *, $P < 0.05$; **, $P < 0.01$ (Student's t test).

with the NGF/TrkA retrograde signaling pathway appears to be tightly associated with Rab5-containing endosomes during PHEV infection.

Ulk1 misdirects NGF/TrkA signaling by promoting Rab5 activation during PHEV infection. Previous work showed that Rab5, acting as a molecular switch of vesicle trafficking, continuously carries out GTP/GDP exchange while functioning (28). To determine whether the state of Rab5 could explain the failure of Ulk1 to support retrograde NGF/TrkA transport and survival, the Ulk1-overexpressed, Ulk1 mutant, and normal neurons were infected with PHEV, lysed, and then tested by a Rab5 GTPase activation assay. In comparison with the normal neurons, the PHEV-infected cortical neurons were found to have strongly increased intrinsic Rab5 GTPase activity in response to Ulk1 restriction (Fig. 7A and B). After transfection of cortical neurons with Ad-Ulk1 followed by PHEV infection, we detected that the phosphorylation of TrkA was significantly increased ($P < 0.017$) by a mean of 3.24 times, but Rab5 GTPase activation was reduced ($P < 0.010$) by a mean of 54.2%, in comparison with the PHEV-infected group (Fig. 7A and B). These Ad-Ulk1-overexpressing neurons that stained for MAP2 also showed enhanced Cy3-fluorescent signals within their growing axons compared with the PHEV-infected or normal neurons, indicating efficient internalization and axonal transport of NGF (Fig. 7C). Furthermore, the opposite results were observed in the Ulk1 mutant neurons, which was in agreement with the PHEV-infected neurons (Fig. 7A and C), suggesting that Ulk1 acts as a positive regulator of NGF/TrkA axonal transport by controlling Rab5 GTPase activation.

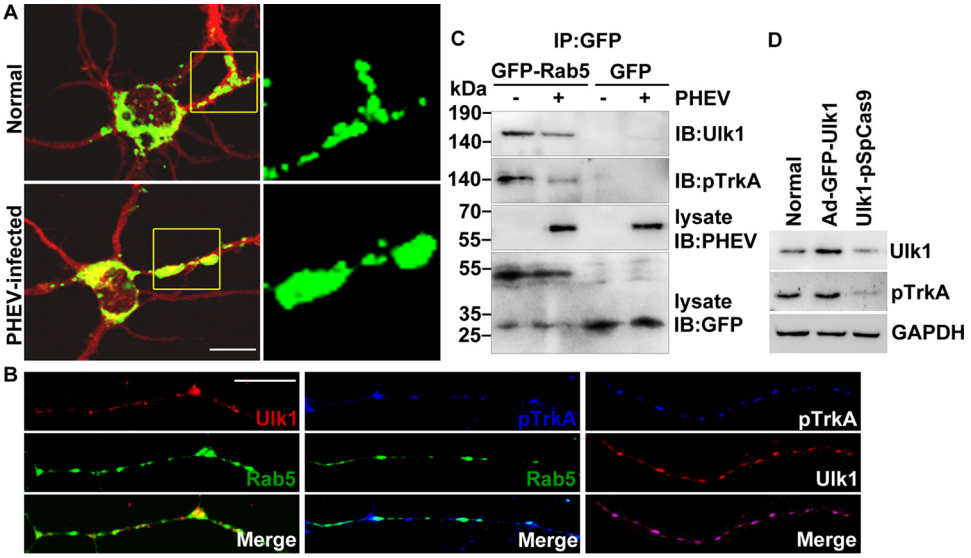

FIG 6 Ulk1 is associated with TrkA within Rab5 endosomes. (A) Cortical neurons were transfected with GFP-Rab5 at 4 DIV for 24 h and incubated with PHEV at 5 DIV for 24 h and then fixed and subjected to immunocytochemistry with an antibody against MAP2 (red). Typical images of GFP-Rab5-expressing neurons are shown in the left panels. Boxed regions are shown at a higher magnification in the right panels. Bar, 20 μm. (B) Cortical neurons (4 DIV) were transfected with GFP-Rab5, fixed, and subjected to immunocytochemistry with antibodies against Ulk1 (red) and pTrkA (blue) at 6 DIV. The representative micrographs showed that the Ulk1 and pTrkA dots were localized along the growing axon within Rab5 endosomes. Bar, 5 μm. (C) GFP-Rab5- or GFP-expressing neurons were infected with PHEV for 24 h, and the cell lysates were immunoprecipitated (IP) by anti-GFP antibody-conjugated Sepharose beads, followed by SDS-PAGE and immunoblot (IB) analysis with the indicated antibodies. (D) With pretreatment of Ad-GFP-Ulk1 transfection or CRISPR/Cas9-mediated Ulk1 mutant in the cortical neurons, the cell lysates were subjected to Western blot assay to determine the levels of Ulk1 and pTrkA.

To further evaluate the relevance of Rab5 in the Ulk1-TrkA-NGF signaling module, we expressed wild-type (GFP-Rab5:wt), constitutively active (GFP-Rab5:Q79L), and dominant negative (GFP-Rab5:S34N) forms of Rab5 in the cortical neurons and then infected them with PHEV for 24 h to depict the effect on neurite outgrowth. We found that the expression level of pTrkA was dramatically decreased in Rab5:Q79L-expressing neurons but enhanced in Rab5:S34N-expressing neurons (Fig. 7D). The total TrkA level of all the transfected neurons was not significantly changed (Fig. 7D). Interestingly, the high-GTPase-activity isoform GFP-Rab5:Q79L facilitated PHEV proliferation in cortical neurons (Fig. 7D). Subsequent microscopic assays revealed that the overexpression of Rab5:Q79L appeared to almost abolish the retrograde transport of pTrkA along the axon, producing a noticeable inhibitory effect on NGF-induced neurite outgrowth (Fig. 7E). In contrast, Rab5:S34N induced a strong appearance of activated pTrkA within dispersed intracellular structures, presumably signaling endosomes, in the soma and the neurites (Fig. 7E). In addition, the NGF/TrkA trafficking was not affected in the GFP-Rab5:S34N-expressing neurons, implying that the activity of Rab5 is essential for the sorting of the NGF/TrkA endosomes to the signaling endosomes and for delivery to the soma. Our findings suggest that dysfunctional Ulk1 misdirects Ulk1-TrkA-NGF signaling of the retrograde transport route in the neurodegeneration process during PHEV infection, which is dependent on Rab5 activity.

DISCUSSION

PHEV is one of five known porcine coronaviruses that cause disease in swine and is considered endemic worldwide, maintaining itself by successively infecting groups of animals after replacement or weaning (10). The virus typically affects pigs <3 weeks of age, and PHEV infections can manifest as two forms of disease: digestive or encephalitic. The encephalitic form of this disease is characterized by progressive weakness and neurological signs, including ataxia, tremors, somnolence, screaming, myoclonus, and flaccid limb paralysis, which make PHEV a deadly encephalitic betacoronavirus. The

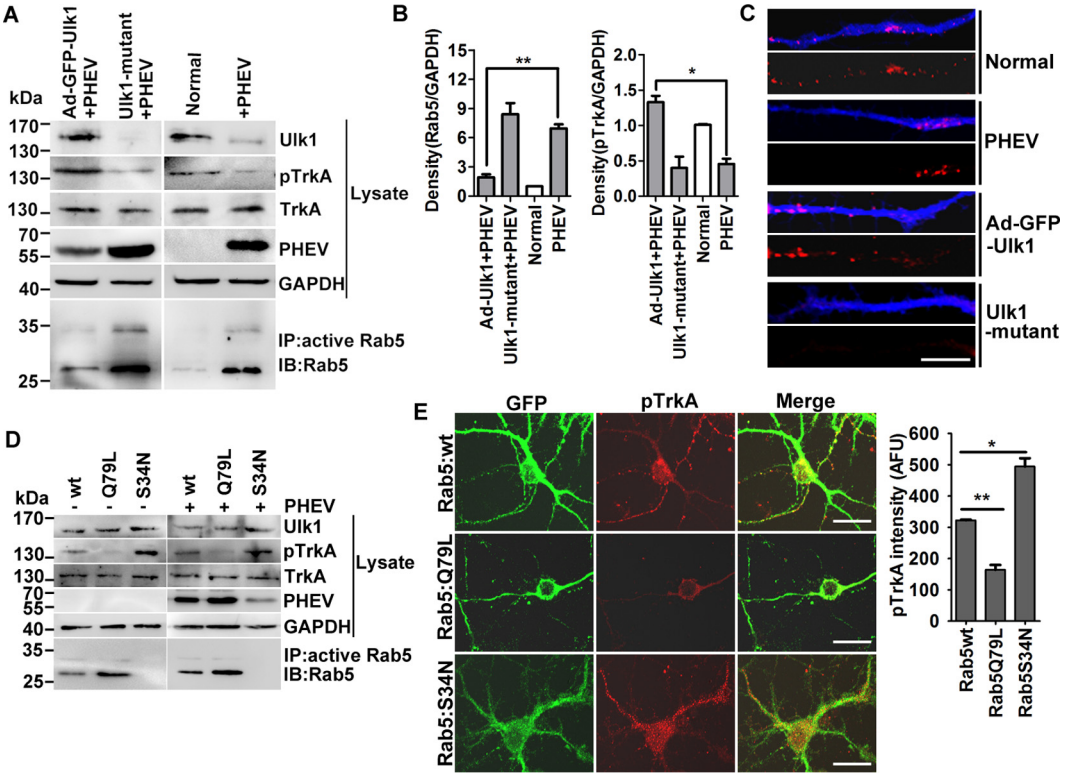

FIG 7 Rab5 GTPase activation blocks Ulk1-mediated NGF/TrkA endocytosis. (A) Ad-GFP-Ulk1-overexpressing or Ulk1 mutant cortical neurons were infected with PHEV for 24 h, and then the cell lysates were subjected to Rab5 activity assays and Western blotting using the indicated antibodies. Immunoprecipitation was performed with the anti-active Rab5 monoclonal antibody (1:500). Immunoblotting was performed with an anti-Rab5 polyclonal antibody (1:1,000). (B) Densitometric analysis of blots in panel A was performed; Rab5 intensities were normalized against GAPDH, and pTrkA intensities were normalized against total TrkA. (C) Differential treatments of the cortical neurons as described for panel A were cultured with standard culture medium containing 10 nM Cy3-NGF (red) for 30 min and then fixed and stained with MAP2 (blue). Representative images were acquired using a confocal microscope. Bars, 20 μm. (D) Cortical neurons were transfected with plasmids encoding Rab5:wt, Rab5:Q79L, or Rab5:S34N at 4 DIV. After 24 h of expression, neurons were infected with PHEV for 24 h and were then harvested for Western blot and Rab5 activity assays using the indicated antibodies. (E) Representative images obtained after GFP-Rab5:wt-, Rab5:Q79L-, or Rab5:S34N-expressing neurons were fixed and stained for pTrkA (red). Bar, 20 μm. Quantification analysis revealed that the pTrkA trafficking was markedly suppressed in the Rab5:Q79L-expressing neurons. The *y* axis represents the average pTrkA intensity per 5 mm of dendrite, and the dendritic field is represented as the sum of the lengths of all the dendrites on one neuron. *, $P < 0.05$; **, $P < 0.01$ (Student's *t* test).

neurologic and digestive characteristics of the disease have been a subject of great interest for many years. PHEV spreads transsynaptically from peripheral nerves to the CNS and infected neurons but not to any glial cells. Its neurotropic properties are similar to those of rabies virus and MHV, indicating that PHEV infection might be a good experimental model for the investigation of control of neurotropic viral infections (7, 29). Further understanding of the mechanisms occurring after the virus has entered the CNS may provide insights into both neurodevelopmental and neurodegenerative diseases, which may lead to targeted approaches for treatment. To date, the underlying neuropathological mechanism of PHEV has yet to be determined. In this context, our findings support a model whereby PHEV infection imposes a physical barrier that restricts the maturation of Rab5 endosomes containing NGF/TrkA into retrograde transport-competent signaling endosomes, and the functional activity of Ulk1 is essential for overcoming this barrier.

Ulk1 is a mammalian homolog of Atg1 and plays key roles in selective and nonselective autophagy induced in response to mitochondrial damage, viral infection, proteotoxic stress, or various forms of metabolic stress (30–32). Mammals have four additional protein kinases that are homologous to Ulk1. They are Ulk2, Ulk3, Ulk4, and STK36 (Ser/Thr kinase 36) and may function redundantly with Ulk1. Mice lacking both

Ulk1 and Ulk2 die within 24 h of birth, implying that these two kinases appear to compensate for the loss of each other (33, 34). Given that PHEV induces autophagy and the appearance of autophagosomes in nerve cells (35), the lack of Ulk1 in the neurons infected with PHEV was surprising. Although we cannot exclude the possibility that another Ulk1 homolog compensates for the lack of Ulk1 in PHEV-infected nerve cells, our findings raise the possibility that Ulk1 is not required for "basal" autophagy in nerve cells. With regard to this issue, recent studies have revealed that the Atg13/FIP200 complex supports starvation-induced neuronal basal autophagy in the absence of Ulk1, expanding the autophagy-independent functions of autophagy proteins (22, 31). However, our data support a primary, autophagy-independent, evolutionarily conserved role for Ulk1 in NGF/TrkA retrograde signaling trafficking that is associated with the neuronal defects observed in PHEV infection. In *Caenorhabditis elegans*, Ulk1 mutations lead to diverse axonal defects, including premature termination, abnormal trajectories, extra axon branches, and abnormal accumulation of intracellular membranous structures (36). Ulk1 directly interacts with Unc-14, which regulates netrin receptor vesicle transport and localization by binding to Unc-16/JIP3/JSAP1, thereby controlling axonal elongation and guidance (37, 38). Ulk1 also interacts with the kinesin-related Vab-8 protein, which regulates cell surface expression of Sax-3/Robo in the growth cones of touch neurons (39). In the mouse, SynGAP and syntenin are modulators of the Rab5-dependent endocytic pathway and have been identified as binding partners for Ulk1 protein (23), suggesting a link between endocytosis and axon growth. The functional importance of Ulk1 in endosomal trafficking is further supported by the finding that Ulk1 protein controls filopodium extension and neurite branching during sensory axon outgrowth, probably by regulating TrkA receptor trafficking and signaling (21). Together with our findings in mouse brain and cultured cortical neurons, these data indicate the significance of Ulk1 in endosomal trafficking, regulating diverse signaling events during axonal elongation, fasciculation, and guidance. Thus, the aberrant neuronal morphogenesis in Ulk1 mutants helps to validate our findings that Ulk1 deficiency is proposed to be the primary cause of neuronal degeneration in the CNS of PHEV-infected mice.

Ulk1 plays an essential role in the delivery of specific receptors for axonal guidance molecules, such as NGF, netrin, SAX-3, and VAB-8 (38–41). Recent studies in isolated sensory neurons have shown that Ulk1 is localized to vesicular structures in growth cones and promotes the endocytic pathway of the neurotrophic tyrosine kinase receptor NGF/TrkA (21). As predicted by the neurotrophic hypothesis, NGF is expressed in target fields of sympathetic neurons and supports their survival and differentiation via long-distance survival signaling (42). The major mechanism by which this long-distance retrograde signaling is carried from the axon terminal to the soma is through NGF-induced internalization of NGF/TrkA complexes and the formation of neurotrophin "signaling endosomes" (43–45). Intriguingly, we noted that Ulk1 puncta, presumably representing the NGF/TrkA-associated endocytic vesicles, do colocalize with Rab5 in the growing axon of cortical neurons. Furthermore, we provide evidence that Ulk1 binds to TrkA in a series of binding assays, the former of which, in turn, binds Rab5 GTPase to tether the Ulk1/TrkA/NGF complex to the vesicular membrane. Taken together with the findings of Liu et al. suggesting that NGF-mediated neurite outgrowth occurs via regulation of Rab5 (24), our findings underscore that Rab5 activity is essential for NGF uptake and for a subsequent step preceding the onset of fast axonal retrograde transport. The TrkA/NGF complexes that are activated at distal sites are, at least in part, internalized and retrograde transported to carry out their biological functions in the soma (46, 47). Despite their physiological importance, the endocytic mechanism controlling the uptake and intracellular trafficking of the TrkA/NGF complex is still controversial.

Previous studies have established a key linkage between Ulk1 function and Rab GTPase signaling, which has previously been shown to act in the neurite outgrowth of some neurons (23, 48). Since long-distance retrograde transport of NGF within signaling endosomes containing Rab5 has a much longer lifetime than in conventional Rab5

early endosomes, this implies that Rab5 activity needs to be suppressed at this stage to divert from the conventional endocytic/degradation pathway. However, we revealed that loss of Ulk1 stimulates the GTPase activity of Rab5 during PHEV infection and leads to truncated neurites and disorganized vesicular compartments in cortical neurons. These results highlight that the Ulk1-containing protein complex governs neuronal morphogenesis by regulating the Rab5 GTPase signaling pathway and the Rab5-dependent endocytic pathway in developing neurons. Recent research on sorting mechanisms has revealed that Rab5-positive endosomes are in fact comprised of two distinct populations: a dynamic population that is highly mobile and matures rapidly into late endosomes and a static population that displays low mobility and matures slowly (49). The latter population resembles the Rab5:S34N-positive structures observed in the cortical neurons used in our study, which show much localized movement and an association with TrkA. The TrkA-containing endosomes with low Rab5 activity are diverted from the early endosomal network (EEN) that is targeted for cargo degradation and, in turn, specialize to become signaling endosomes that serve as a platform for signaling processes leading to neurite outgrowth and differentiation. In agreement with this possibility, our findings raise the possibility that an Ulk1/TrkA/NGF complex regulates the PHEV-mediated turnover of neuronal degeneration in a Rab5 GTPase-dependent manner.

The main findings of this study are supported by a series of experimental results. First, PHEV infection inhibited the expression of Ulk1 protein and resulted in increased Rab5 GTPase activation in the cortical neurons, whereas Rab5 signaling is normally attenuated by functional Ulk1 in healthy neurons. Second, Ulk1 cross talk with the NGF receptor TrkA appeared to facilitate translocation into Rab5 endosomes, and this physical coupling can prevent TrkA-containing endosomes from entering the EEN by Rab5 GTPase inactivation, but there is a loss of control in Ulk1 deficiency. Third, high Rab5 activity diminishes intracellular NGF signaling by rapid dephosphorylation of internalized pTrkA, possibly via gaining access to endosomal fusion at this stage in the conventional endocytic/degradation pathway. Finally, Rab5 endosomes containing the NGF/TrkA complex fail to mature into signaling endosomes for sustained long-distance retrograde transport, explaining the failure of neurite outgrowth and a possible degenerating process induced by PHEV. Whereas elucidation of the exact molecular components that are involved in PHEV-induced neurodegeneration is an important subject for future studies, our study defines a mechanistic link between alterations in signaling in endocytic pathways and the neuropathogenesis involved in PHEV-induced CNS disorders.

The PHEV virion typically encodes 5 structural proteins: hemagglutinin-esterase (HE), spike (S), small membrane (E), membrane (M), and nucleocapsid (N). The HE protein is a membrane envelope and forms a second set of small spikes that assist in the attachment of virus to host cells and prevent aggregation of progeny virions (50). Notably, in infections of mice, it was found that the presence of HE dramatically enhanced neurovirulence, as measured by viral spread and lethality (51). Thus, the HE protein provides an advantage to the virus *in vivo* and may be supposed to be involved in the Rab5 pathway and affect the formation of retrograde signaling endosomes in PHEV-induced CNS disorder. Future work is needed to further characterize the cellular and viral factors of the Ulk1-mediated endocytic processes, as well as the fates of the Ulk1-mediated endocytosed NGF/TrkA vesicles. Suffice it to say, our study does highlight the importance of endocytic processes in regulating trophic signaling events during neuronal morphogenesis.

MATERIALS AND METHODS

Animal protocols and ethics statement. For the establishment of an animal infection model, 3-week-old BALB/c mice (male) were intranasally inoculated with PHEV ($10^{4.45}$ 50% tissue culture infectious doses [$TCID_{50}$]/0.1 ml), while mice in the negative-control group were treated with equal amounts of phosphate-buffered saline (PBS, 1 M, pH 7.4). Clinical signs were monitored and recorded daily. Following anesthetization of the mice with 3.5% chloral hydrate (1.0 ml/100 g; Sigma, USA) at various time points, brain tissue was collected and fixed. This study was approved by the Institutional

Animal Care and Use Committee of the College of Veterinary Medicine, Jilin University, China (permission number 2012-CVM-12) and was performed in accordance with the guidelines of the International Guiding Principles for Biomedical Research Involving Animals, as revised by the International Council for Laboratory Animal Science (ICLAS) and the Councils for International Organizations of Medical Sciences (CIOMS).

Virus, plasmids, reagents, and antibodies. The PHEV strain used in this study was HEV 67N (GenBank accession number AY078417), which was previously kept by our research group. The cDNAs of Rab5:wt (wild type), Rab5:Q79L, and Rab5:S34N were generated by PCR and subcloned into pEGFP-N1 vectors. Monoclonal antibodies (MAbs) for Rab5, Ulk1, TrkA, phospho-TrkA (pTrkA), and microtubule-associated protein 2 (MAP2) were purchased from Cell Signaling Technology (Beverly, MA). The natural mouse nerve growth factor 2.5S (NGF 2.5S) was obtained from Invitrogen Corporation. The mouse anti-PHEV-S MAb 1E2, replication-deficient adenovirus-based green fluorescent protein expression vectors (Ad-GFP), and Ad-GFP-Ulk1 were kindly provided by our research support group.

Primary cultures of rat cortical neurons. Cortical neurons from newborn (P0) rats were isolated as described previously. Primary cortical neurons were maintained in neurobasal medium containing 1% B27 supplement, 0.5 mM L-glutamine, and 10 U/ml penicillin-streptomycin (Invitrogen, Gaithersburg, MD) and seeded on plates coated with poly–D-lysine (Sigma, St. Louis, MO). For transfection, the neurons were transfected with the indicated plasmids by using X-tremeGENE HP DNA transfection reagent (Roche, Sweden) according to the manufacturer's protocol.

Quantitative reverse transcription-PCR assay. For qRT-PCR, total RNA was extracted using TRIzol Reagent (Invitrogen), and reverse transcription was performed using PrimeScript reverse transcriptase (TaKaRa, Japan). Quantitative PCRs were conducted with SYBR Premix Ex TaqTM II (TaKaRa, Japan) to analyze Ulk1 expression, with GAPDH (glyceraldehyde-3-phosphate dehydrogenase) as a housekeeping gene for the purpose of normalization. The primers for Ulk1 and GAPDH were designed as follows: Ulk1 sense primer, 5′-ACTTTGGATTCGCTCGGTAC-3′; Ulk1 antisense primer, 5′-GGTCAGCCTTTCCATCGTAG-3′; GAPDH sense primer, 5′-CTCAACTACATGGTCTACATGTTC-3′; GAPDH antisense primer, 5′-ATTTGATGTT AGTGGGGTCTCGCTC-3′. The qRT-PCR conditions were predegeneration at 95°C for 3 min, denaturation at 95°C for 30 s, annealing at 60°C for 30 s, and extension at 72°C for 30 s with a total of 40 cycles.

Histopathologic examination. For H&E staining, paraffin-embedded brain tissues slides were dewaxed, hydrated, and stained in alum hematoxylin for 5 min, followed by washing and coloring for 30 s in eosin, followed by dehydration, processing for transparency, and mounting with neutral balsam. For the immunohistochemistry testing, the paraffin slides were incubated with the primary antibody (1:100) overnight at 4°C after heat-mediated antigen retrieval and were subsequently incubated with peroxidase-labeled anti-mouse antibody at 37°C for 1 h, followed by staining for 10 min with diaminobenzidine (DAB; Sigma-Aldrich Chemical Company, St. Louis MO, USA) and restaining with hematoxylin. Negative controls were incubated with PBS instead of antibodies.

Immunofluorescence staining. For immunofluorescence staining, cultured cortical neurons were rinsed three times with PBS and fixed for 10 min with 4% paraformaldehyde at room temperature, followed by permeabilization with 0.2% Triton X-100 for 10 min. Immunostaining was performed by using primary antibodies (i.e., MAP2, Ulk1, TrkA, pTrkA, PHEV) overnight at 4°C and subsequent incubation with secondary antibodies conjugated with either Alexa Fluor 488 or Alexa Fluor 594 (1:1,000) for 1 h at room temperature. Following counterstaining with 4′,6-diamidino-2-phenylindole (DAPI, 1:5,000; Sigma) for 5 min at room temperature, coverslips were mounted before viewing with a confocal microscope (FV10-ASW 3.0; Olympus Europa Holding GmbH). For staining of brain tissues, the slides were dewaxed, immersed in blocking buffer (10% serum and 0.1% Triton X-100 in PBS) for 1 h at room temperature, stained with primary antibodies and fluorescent secondary antibodies before counterstaining, and then processed for microscopy analysis.

***In situ* hybridization.** Frozen sections were fixed with 4% paraformaldehyde–diethyl pyrocarbonate (DEPC)–PBS, treated with 0.25% acetic anhydride in 0.1 M triethanolamine (TEA) for 10 min, and washed in PBS. Hybridization with digoxigenin (DIG)-labeled mRNA probes (Exonbio, Guangzhou, China) was performed in hybridization buffer at 42°C overnight. After blocking in TNB blocking buffer (DuPont NEN, Boston, MA) for 30 min at room temperature, aminomethylcoumarin (AMCA)-conjugated anti-DIG antibody (Exonbio, Guangzhou, China) was applied for 1 h at 37°C (in the dark), followed by counterstaining with DAPI at room temperature for 5 min. Image acquisition was performed on a confocal microscope with an appropriate filter set. The following primer was designed to amplify the antisense probe: 5′-CCAGGAAAGTGTGGTGGC-3′.

Cy3-NGF internalization assay. Primary cortical neurons were first cultured for 48 h with standard culture medium containing 1 nM NGF. Then, the culture medium was replaced with fresh medium containing 10 nM Cy3-NGF (prewarmed to 37°C) and incubated for 10 min. The medium was replaced again with standard culture medium containing unlabeled NGF (1 nM) for an additional 10 min at 37°C. Afterward, the culture chambers were placed on ice, washed, fixed, and stained. The total Cy3 fluorescence was acquired using a confocal microscope and measured for each growth neurite to obtain a measurement of the average fluorescence per pixel expressed as an arbitrary fluorescence unit (AFU). Representative images were analyzed using the ImageJ plugin Neuron J.

Coimmunoprecipitation assay. For co-IP assays, following transfection with/without PHEV infection as indicated, the cells were allowed to recover in full growth medium and to express the recombinant proteins for 24 h at 37°C. The cells were then rinsed with ice-cold PBS and lysed in lysis buffer (20 mM Tris-HCl [pH 7.4], 150 mM NaCl, 1% Triton X-100, 2 mM sodium orthovanadate, 2 mM para-nitrophenol phosphate, and protease inhibitor) for 45 min on ice. After clearing at 10,000 $\times$ *g* for 15 min, the cell lysates were incubated with anti-GFP antibody-conjugated Sepharose beads (Abcam) overnight at 4°C.

The beads were then washed 5 times with the lysis buffer and boiled for 5 min in SDS sample buffer, followed by immunoblot analysis with anti-TrkA, anti-Ulk1, anti-Rab5, and anti-GFP antibodies.

CRISPR/Cas9 plasmid design. For targeting the endogenous Ulk1 gene, two sgRNAs were designed and cloned into a pSpCas9 (BB)-2A-Puro vector; a schematic of the expression cassette in the single-plasmid system is shown in Fig. 2B. The sgRNA complexes with Cas9 were used to mediate cleavage of the target DNA sites that were complementary to the 20 nucleotides (nt) of the guide RNA and lay next to a protospacer adjacent motif (PAM) sequence. The position of the frameshift of the CRISPR-Cas9 knockout was located at exon 2 within the Ulk1 gene, and the guide RNA sequence (including PAM) is as follows: TGCATTTGACGGCCACCTCCAGG. Plasmid purification and transfection were performed with X-tremeGENE HP DNA transfection reagent (Roche, Sweden) according to the manufacturer's protocol. Detection of the target mutations was performed by T7 endonuclease I (T7E1) assay and PCR Sanger sequencing.

Rab5 GTPase activation assays. For Rab5 GTPase activation assays, the cells were stimulated with PHEV as desired, and the Rab5 GTP level was measured 24 h later with a Rab5 activation assay kit (NewEast Biosciences, Malvern, PA) according to the manufacturer's instructions. Briefly, the cells were washed twice with ice-cold PBS and lysed in an ice-cold 1× assay/lysis buffer for 20 min on ice. The lysates were transferred to appropriately sized tubes and cleared at 12,000 × *g* for 10 min at 4°C. The supernatants were then collected to a microcentrifuge tube, and anti-active Rab5 MAb (1:1,000) and 20 μl of resuspended bead slurry were added. The tubes were incubated at 4°C for 1 h with gentle agitation, followed by aspiration and discarding of the supernatant by centrifugation for 1 min at 5,000 × *g*. We then resuspended the bead pellet in reducing SDS-PAGE sample buffer, boiled it for 5 min, and then processed it for SDS-PAGE and immunoblotting detection.

Statistical analyses. Statistical analysis was performed with either Student's *t* test or one-way analysis of variance (ANOVA) in GraphPad Prism version 5 software. A *P* value of <0.05 was defined as the threshold for statistical significance.

ACKNOWLEDGMENTS

This study was supported by the National Key Research and Development Program of China (grant 2016YFD0500102), the National Natural Science Foundation of China (grants 31672519, 31772704, and 31602018), and the Scientific and Technological Project of Jilin Province (grants 20180101270JC, 20170204033NY, and 20160520033JH).

The funders had no role in study design, data collection and interpretation, or the decision to submit the work for publication.

We declare that we have no conflicts of interest.

Z.L. and W.H. designed and supervised the experiments. Z.L. and K.Z. performed most of the experiments and interpreted the data. X.L. and Y.L. cultured neurons and analyzed the confocal laser scanning images. H.L., H.H., and F.G. made ultrathin sections and analyzed them by TEM. S.H. and Y.Y. constructed plasmids. J.G. and J.S. carried out the co-IP test and prepared the figures. Z.L. drafted the article, and F.G. and W.H. revised it critically for important intellectual content.

REFERENCES

1. Greig AS, Mitchell D, Corner AH, Bannister GL, Meads EB, Julian RJ. 1962. A hemagglutinating virus producing encephalomyelitis in baby pigs. Can J Comp Med Vet Sci 26:49–56.
2. Vijgen L, Keyaerts E, Lemey P, Maes P, Van Reeth K, Nauwynck H, Pensaert M, Van Ranst M. 2006. Evolutionary history of the closely related group 2 coronaviruses: porcine hemagglutinating encephalomyelitis virus, bovine coronavirus, and human coronavirus OC43. J Virol 80:7270–7274. https://doi.org/10.1128/JVI.02675-05.
3. Alsop JE. 2006. A presumptive case of vomiting and wasting disease in a swine nucleus herd. J Swine Health Production 14:97–100.
4. Quiroga MA, Cappuccio J, Pineyro P, Basso W, More G, Kienast M, Schonfeld S, Cancer JL, Arauz S, Pintos ME, Nanni M, Machuca M, Hirano N, Perfumo CJ. 2008. Hemagglutinating encephalomyelitis coronavirus infection in pigs, Argentina. Emerg Infect Dis 14:484–486. https://doi.org/10.3201/eid1403.070825.
5. Mengeling WL. 1975. Incidence of antibody for hemagglutinating encephalomyelitis virus in serums from swine in the United States. Am J Vet Res 36:821–823.
6. Li Z, He W, Lan Y, Zhao K, Lv X, Lu H, Ding N, Zhang J, Shi J, Shan C, Gao F. 2016. The evidence of porcine hemagglutinating encephalomyelitis virus induced nonsuppurative encephalitis as the cause of death in piglets. PeerJ 4:e2443. https://doi.org/10.7717/peerj.2443.
7. Hirano N, Haga S, Sada Y, Tohyama K. 2001. Susceptibility of rats of different ages to inoculation with swine haemagglutinating encephalomyelitis virus (a coronavirus) by various routes. J Comp Pathol 125:8–14. https://doi.org/10.1053/jcpa.2001.0471.
8. Li Z, Zhao K, Lan Y, Lv X, Hu S, Guan J, Lu H, Zhang J, Shi J, Yang Y, Song D, Gao F, He W. 2017. Porcine hemagglutinating encephalomyelitis virus enters Neuro-2a cells via clathrin-mediated endocytosis in a Rab5-, cholesterol-, and pH-dependent manner. J Virol 91:e01083-17. https://doi.org/10.1128/JVI.01083-17.
9. Li YC, Bai WZ, Hirano N, Hayashida T, Taniguchi T, Sugita Y, Tohyama K, Hashikawa T. 2013. Neurotropic virus tracing suggests a membranous-coating-mediated mechanism for transsynaptic communication. J Comp Neurol 521:203–212. https://doi.org/10.1002/cne.23171.
10. Lorbach JN, Wang L, Nolting JM, Benjamin MG, Killian ML, Zhang Y, Bowman AS. 2017. Porcine hemagglutinating encephalomyelitis virus and respiratory disease in exhibition swine, Michigan, USA, 2015. Emerg Infect Dis 23:1168–1171. https://doi.org/10.3201/eid2307.170019.
11. Buchmeier MJ, Lane TE. 1999. Viral-induced neurodegenerative disease. Curr Opin Microbiol 2:398–402. https://doi.org/10.1016/S1369-5274(99)80070-8.
12. Ludlow M, Kortekaas J, Herden C, Hoffmann B, Tappe D, Trebst C, Griffin DE, Brindle HE, Solomon T, Brown AS, van Riel D, Wolthers KC, Pajkrt D, Wohlsein P, Martina BEE, Baumgartner W, Verjans GM, Osterhaus ADME. 2016. Neurotropic virus infections as the cause of immediate and delayed neuropathology. Acta Neuropathol 131:159–184. https://doi.org/10.1007/s00401-015-1511-3.

13. Oleszak EL, Chang JR, Friedman H, Katsetos CD, Platsoucas CD. 2004. Theiler's virus infection: a model for multiple sclerosis. Clin Microbiol Rev 17:174–207. https://doi.org/10.1128/CMR.17.1.174-207.2004.
14. Schneider R. 2009. Neuronal degeneration in a viral model of multiple sclerosis. J Neurosci 29:15353–15354. https://doi.org/10.1523/JNEUROSCI.5198-09.2009.
15. Das Sarma J, Kenyon LC, Hingley ST, Shindler KS. 2009. Mechanisms of primary axonal damage in a viral model of multiple sclerosis. J Neurosci 29:10272–10280. https://doi.org/10.1523/JNEUROSCI.1975-09.2009.
16. Hardy J, Gwinn-Hardy K. 1998. Genetic classification of primary neurodegenerative disease. Science 282:1075–1079. https://doi.org/10.1126/science.282.5391.1075.
17. Urdinguio RG, Sanchez-Mut JV, Esteller M. 2009. Epigenetic mechanisms in neurological diseases: genes, syndromes, and therapies. Lancet Neurol 8:1056–1072. https://doi.org/10.1016/S1474-4422(09)70262-5.
18. Lan Y, Zhao K, Zhao J, Lv X, Wang G, Lu H, Tang B, Li Z, Chang L, Jin Z, He W, Gao F. 2014. Gene-expression patterns in the cerebral cortex of mice infected with porcine haemagglutinating encephalomyelitis virus detected using microarray. J Gen Virol 95:2192–2203. https://doi.org/10.1099/vir.0.066845-0.
19. Toda H, Mochizuki H, Flores R, III, Josowitz R, Krasieva TB, Lamorte VJ, Suzuki E, Gindhart JG, Furukubo-Tokunaga K, Tomoda T. 2008. UNC-51/ATG1 kinase regulates axonal transport by mediating motor-cargo assembly. Genes Dev 22:3292–3307. https://doi.org/10.1101/gad.1734608.
20. Mochizuki H, Toda H, Ando M, Kurusu M, Tomoda T, Furukubo-Tokunaga K. 2011. Unc-51/ATG1 controls axonal and dendritic development via kinesin-mediated vesicle transport in the Drosophila brain. PLoS One 6:e19632. https://doi.org/10.1371/journal.pone.0019632.
21. Zhou X, Babu JR, da Silva S, Shu Q, Graef IA, Oliver T, Tomoda T, Tani T, Wooten MW, Wang F. 2007. Unc-51-like kinase 1/2-mediated endocytic processes regulate filopodia extension and branching of sensory axons. Proc Natl Acad Sci U S A 104:5842–5847. https://doi.org/10.1073/pnas.0701402104.
22. Zhao YG, Zhang H. 2016. The incredible ULKs: autophagy and beyond. Mol Cell 62:475–476. https://doi.org/10.1016/j.molcel.2016.05.005.
23. Tomoda T, Kim JH, Zhan C, Hatten ME. 2004. Role of Unc51.1 and its binding partners in CNS axon outgrowth. Genes Dev 18:541–558. https://doi.org/10.1101/gad.1151204.
24. Liu J, Lamb D, Chou MM, Liu YJ, Li G. 2007. Nerve growth factor-mediated neurite outgrowth via regulation of Rab5. Mol Biol Cell 18:1375–1384. https://doi.org/10.1091/mbc.e06-08-0725.
25. Raab-Traub N, Dittmer DP. 2017. Viral effects on the content and function of extracellular vesicles. Nat Rev Microbiol 15:559–572. https://doi.org/10.1038/nrmicro.2017.60.
26. Joo JH, Wang B, Frankel E, Ge L, Xu L, Iyengar R, Li-Harms X, Wright C, Shaw TI, Lindsten T, Green DR, Peng JM, Hendershot LM, Kilic F, Sze JY, Audhya A, Kundu M. 2016. The noncanonical role of ULK/ATG1 in ER-to-Golgi trafficking is essential for cellular homeostasis. Mol Cell 62:491–506. https://doi.org/10.1016/j.molcel.2016.04.020.
27. Villarroel-Campos D, Gastaldi L, Conde C, Caceres A, Gonzalez-Billault C. 2014. Rab-mediated trafficking role in neurite formation. J Neurochem 129:240–248. https://doi.org/10.1111/jnc.12676.
28. Carney DS, Davies BA, Horazdovsky BF. 2006. Vps9 domain-containing proteins: activators of Rab5 GTPases from yeast to neurons. Trends Cell Biol 16:27–35. https://doi.org/10.1016/j.tcb.2005.11.001.
29. Hirano N, Nomura R, Tawara T, Tohyama K. 2004. Neurotropism of swine haemagglutinating encephalomyelitis virus (coronavirus) in mice depending upon host age and route of infection. J Comp Pathol 130:58–65. https://doi.org/10.1016/S0021-9975(03)00083-5.
30. Noda NN, Fujioka Y. 2015. Atg1 family kinases in autophagy initiation. Cell Mol Life Sci 72:3083–3096. https://doi.org/10.1007/s00018-015-1917-z.
31. Joo JH, Dorsey FC, Joshi A, Hennessy-Walters KM, Rose KL, McCastlain K, Zhang J, Iyengar R, Jung CH, Suen DF, Steeves MA, Yang CY, Prater SM, Kim DH, Thompson CB, Youle RJ, Ney PA, Cleveland JL, Kundu M. 2011. Hsp90-Cdc37 chaperone complex regulates Ulk1- and Atg13-mediated mitophagy. Mol Cell 43:572–585. https://doi.org/10.1016/j.molcel.2011.06.018.
32. Hieke N, Loffler AS, Kaizuka T, Berleth N, Bohler P, Driessen S, Stuhldreier F, Friesen O, Assani K, Schmitz K, Peter C, Diedrich B, Dengjel J, Holland P, Simonsen A, Wesselborg S, Mizushima N, Stork B. 2015. Expression of a ULK1/2 binding-deficient ATG13 variant can partially restore autophagic activity in ATG13-deficient cells. Autophagy 11:1471–1483. https://doi.org/10.1080/15548627.2015.1068488.
33. Lee EJ, Tournier C. 2011. The requirement of uncoordinated 51-like kinase 1 (ULK1) and ULK2 in the regulation of autophagy. Autophagy 7:689–695. https://doi.org/10.4161/auto.7.7.15450.
34. Cheong H, Lindsten T, Wu J, Lu C, Thompson CB. 2011. Ammonia-induced autophagy is independent of ULK1/ULK2 kinases. Proc Natl Acad Sci U S A 108:11121–11126. https://doi.org/10.1073/pnas.1107969108.
35. Ding N, Zhao K, Lan Y, Li Z, Lv X, Su J, Lu H, Gao F, He W. 2017. Induction of atypical autophagy by porcine hemagglutinating encephalomyelitis virus contributes to viral replication. Front Cell Infect Microbiol 7:56. https://doi.org/10.3389/fcimb.2017.00056.
36. Ogura K, Wicky C, Magnenat L, Tobler H, Mori I, Muller F, Ohshima Y. 1994. Caenorhabditis elegans unc-51 gene required for axonal elongation encodes a novel serine/threonine kinase. Genes Dev 8:2389–2400. https://doi.org/10.1101/gad.8.20.2389.
37. Sakamoto R, Byrd DT, Brown HM, Hisamoto N, Matsumoto K, Jin Y. 2005. The Caenorhabditis elegans UNC-14 RUN domain protein binds to the kinesin-1 and UNC-16 complex and regulates synaptic vesicle localization. Mol Biol Cell 16:483–496. https://doi.org/10.1091/mbc.e04-07-0553.
38. Ogura K, Goshima Y. 2006. The autophagy-related kinase UNC-51 and its binding partner UNC-14 regulate the subcellular localization of the Netrin receptor UNC-5 in Caenorhabditis elegans. Development 133:3441–3450. https://doi.org/10.1242/dev.02503.
39. Watari-Goshima N, Ogura K, Wolf FW, Goshima Y, Garriga G. 2007. C. elegans VAB-8 and UNC-73 regulate the SAX-3 receptor to direct cell and growth-cone migrations. Nat Neurosci 10:169–176. https://doi.org/10.1038/nn1834.
40. Levy-Strumpf N, Culotti JG. 2007. VAB-8, UNC-73 and MIG-2 regulate axon polarity and cell migration functions of UNC-40 in C. elegans. Nat Neurosci 10:161–168. https://doi.org/10.1038/nn1835.
41. Xu Y, Taru H, Jin Y, Quinn CC. 2015. SYD-1C, UNC-40 (DCC) and SAX-3 (Robo) function interdependently to promote axon guidance by regulating the MIG-2 GTPase. PLoS Genet 11:e1005185. https://doi.org/10.1371/journal.pgen.1005185.
42. Aloe L, Rocco ML, Balzamino BO, Micera A. 2015. Nerve growth factor: a focus on neuroscience and therapy. Curr Neuropharmacol 13:294–303. https://doi.org/10.2174/1570159X13666150403231920.
43. Harrington AW, St Hillaire C, Zweifel LS, Glebova NO, Philippidou P, Halegoua S, Ginty DD. 2011. Recruitment of actin modifiers to TrkA endosomes governs retrograde NGF signaling and survival. Cell 146:421–434. https://doi.org/10.1016/j.cell.2011.07.008.
44. Sharma N, Deppmann CD, Harrington AW, St Hillaire C, Chen ZY, Lee FS, Ginty DD. 2010. Long-distance control of synapse assembly by target-derived NGF. Neuron 67:422–434. https://doi.org/10.1016/j.neuron.2010.07.018.
45. Pazyra-Murphy MF, Hans A, Courchesne SL, Karch C, Cosker KE, Heerssen HM, Watson FL, Kim T, Greenberg ME, Segal RA. 2009. A retrograde neuronal survival response: target-derived neurotrophins regulate MEF2D and bcl-w. J Neurosci 29:6700–6709. https://doi.org/10.1523/JNEUROSCI.0233-09.2009.
46. Delcroix JD, Valletta JS, Wu CB, Hunt SJ, Kowal AS, Mobley WC. 2003. NGF signaling in sensory neurons: Evidence that early endosomes carry NGF retrograde signals. Neuron 39:69–84. https://doi.org/10.1016/S0896-6273(03)00397-0.
47. Newbern JM, Li X, Snider WD. 2010. Signaling endosomes trigger synapse assembly. Neuron 67:352–354. https://doi.org/10.1016/j.neuron.2010.07.025.
48. Eggert A, Ikegaki N, Liu X, Chou TT, Lee VM, Trojanowski JQ, Brodeur GM. 2000. Molecular dissection of TrkA signal transduction pathways mediating differentiation in human neuroblastoma cells. Oncogene 19:2043–2051. https://doi.org/10.1038/sj.onc.1203518.
49. Lakadamyali M, Rust MJ, Zhuang XW. 2006. Ligands for clathrin-mediated endocytosis are differentially sorted into distinct populations of early endosomes. Cell 124:997–1009. https://doi.org/10.1016/j.cell.2005.12.038.
50. Masters PS. 2006. The molecular biology of coronaviruses. Adv Virus Res 66:193–292. https://doi.org/10.1016/S0065-3527(06)66005-3.
51. Kazi L, Lissenberg A, Watson R, de Groot RJ, Weiss SR. 2005. Expression of hemagglutinin esterase protein from recombinant mouse hepatitis virus enhances neurovirulence. J Virol 79:15064–15073. https://doi.org/10.1128/JVI.79.24.15064-15073.2005.